# Positionally heterogeneous non-fully conjugated dimeric acceptors with unilateral conjugated π-bridge enable highly efficient and stable organic solar cells

## 1. Experimental Section

### Materials and Synthesis

All reagents and chemicals were purchased from Energy Chemical. bide, etc. All reagents and chemicals were used as received without further purification unless otherwise specified. The 1,6-Bis(5-(trimethylstannyl)thiophen-2-yl)hexane from Derthon. The 2-(5,6-difluoro-3-oxo-2,3-dihydro-1H-inden-1-ylidene) malononitrile(2F-IC) and 2-(5-Bromo-2,3-dihydro-3-oxo-1H-inden-1-ylidene)propanedinitrile(Br-IC) was purchased from HWRK Chem Co., Ltd. 2,9-bis(2-((2-hydroxyethyl)amino)ethyl)anthra[2,1,9-def:6,5,10-d'e'f']diisoquinoline-1,3,8,10(2H,9H)-tetraone(PDI N-OH), 1-Bromo-3,5-dichlorobenzene(DCBB), (4-(3,6-diphenyl-9H-carbazol-9-yl)butyl)phosphonic(PH-4PACZ), tributyl(1,3-dioxolan-2-ylmethyl)phosphonium bromide and others were all purchased from regular reagent suppliers on the market and used directly without further processing. The ITO substrate was purchased from ZaoFu Technology and etched to 6.2 mm. Both DY-TC6T-V-out and DY-TC6T-V-in were synthesized according to previously reported literature methods.[1, 2] The detailed synthetic procedures of these compounds and polymers are shown as followings.

### The synthetic path of DY-TC6T-V-out and DY-TC6T-V-in

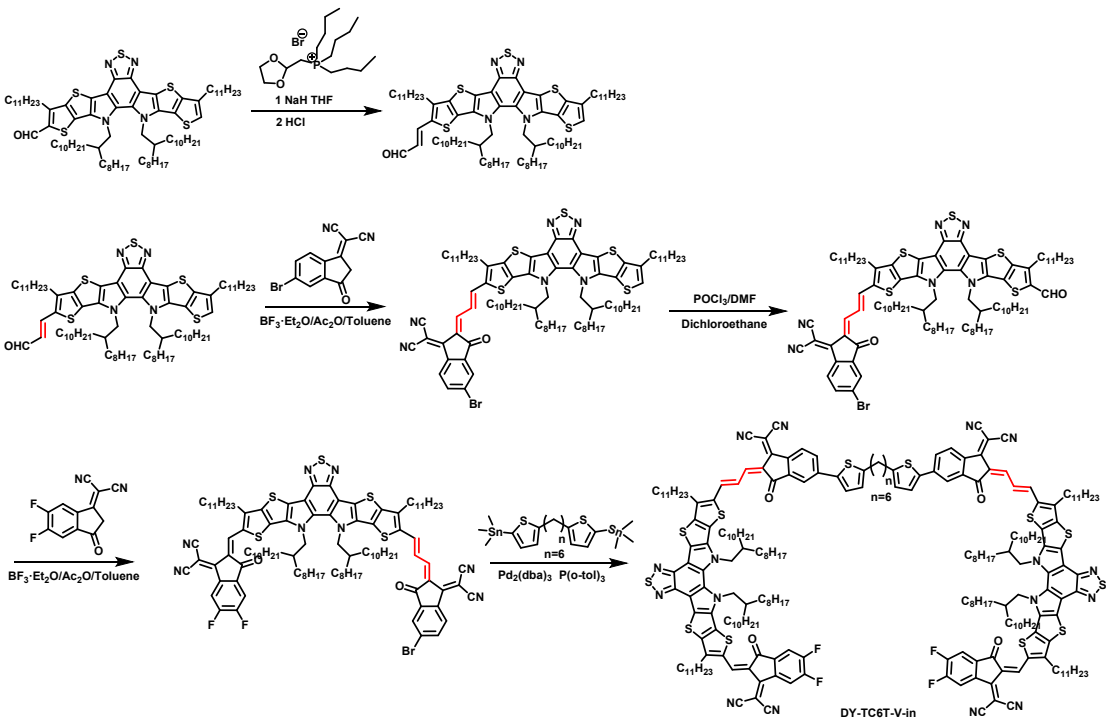

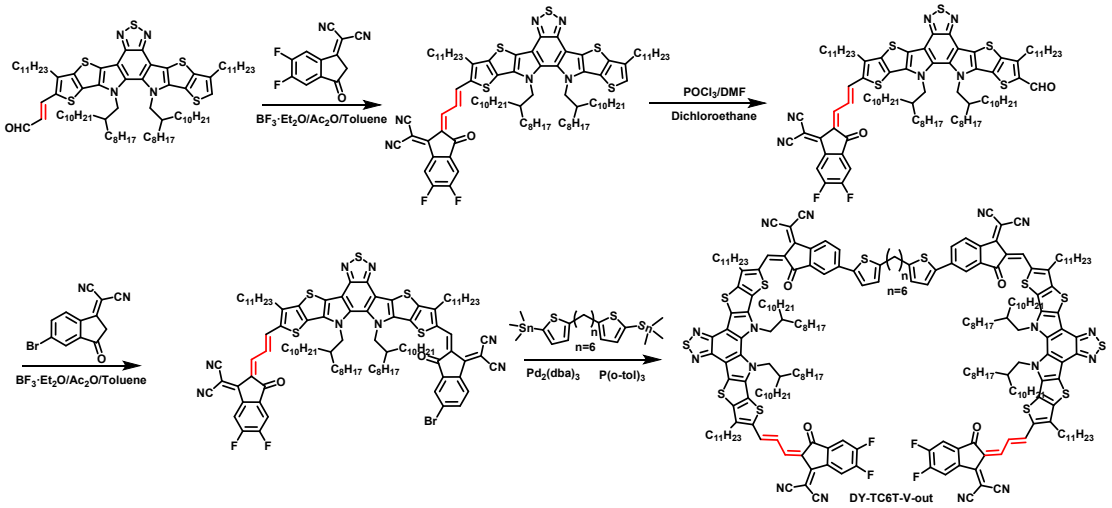


**Figure S1.** The synthetic path of DY-TC6T-V-out and DY-TC6T-V-in.

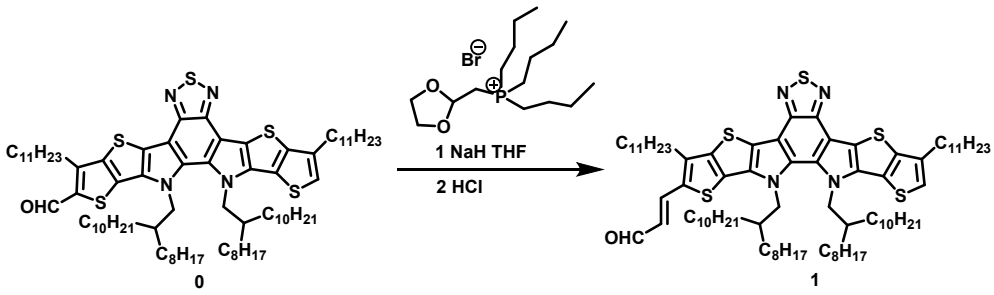


**Figure S2.** Synthesis of compound **1**.

Under an argon atmosphere, compound 0(0.256g 0.192mmol), tributyl(1,3-dioxolan-2-ylmethyl)phosphonium bromide(0.078mg 0.211mmol), and sodium hydride(60% dispersed in mineral oil 0.576mmol) were added to a three-neck flask containing anhydrous tetrahydrofuran(20ml). The mixture was stirred at room temperature for 24 hours. Subsequently, 10% hydrochloric acid was introduced into the reaction vessel to acidify the mixture. After stirring for 4 to 5 hours, the product was extracted and concentrated using dichloromethane and water. The organic phase was collected and purified by column chromatography to yield compound 1(0.205g, yield 78%). $^1$H NMR (400 MHz, Chloroform-d) $\delta$ 9.69 (d, J = 7.6 Hz, 1H), 7.77 (d, J = 15.3 Hz, 1H), 7.04 (s, 1H), 6.51 (dd, J = 15.2, 7.6 Hz, 1H), 4.59 (d, J = 7.8 Hz, 4H), 2.98 (t, J = 7.8 Hz, 2H), 2.82 (t, J = 7.8 Hz, 2H), 2.05 (d, J = 13.2 Hz, 3H), 1.86 (p, J = 7.6 Hz, 5H), 1.52 – 1.34 (m, 7H), 1.34 – 1.08 (m, 47H), 1.08 – 0.63 (m, 74H).

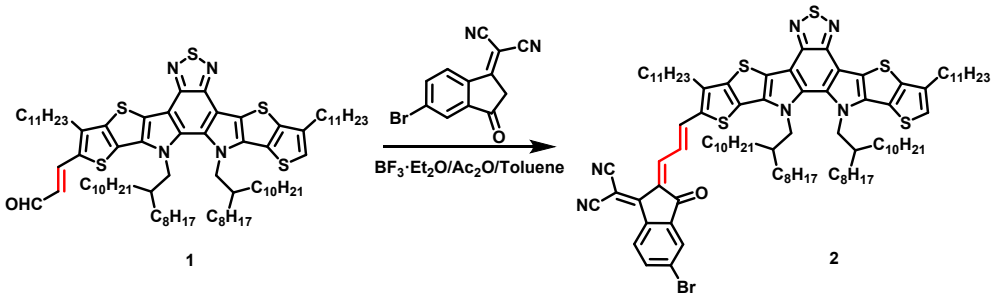


**Figure S3.** Synthesis of compound **2**.

To the flask was added compound **1**(0.400 g 0.294 mmol), Br-IC(0.088 g 0.324 mmol), $BF_3$·$Et_2O$(0.1 mL), $Ac_2O$(0.2 mL) and toluene(20 mL). After stirring for 10 mins, the reaction solution was poured into methanol and filtered.

The compound **2** was obtained by column chromatography(PE:DCM=3:1). Dark green solid(0.314 g, yield 66%). $^1$H NMR (400 MHz, Chloroform-d) δ 8.64 (dd, J = 14.1, 11.8 Hz, 1H), 8.58 – 8.48 (m, 2H), 7.98 (d, J = 1.9 Hz, 1H), 7.85 (dd, J = 8.4, 2.0 Hz, 1H), 7.74 (d, J = 14.1 Hz, 1H), 7.08 (s, 1H), 4.61 (d, J = 7.7 Hz, 4H), 3.02 (t, J = 7.8 Hz, 2H), 2.83 (t, J = 7.8 Hz, 2H), 2.16 – 1.95 (m, 2H), 1.85 (d, J = 9.3 Hz, 4H), 1.55 (s, 8H), 1.27 (q, J = 6.9, 4.7 Hz, 34H), 1.20 – 0.90 (m, 69H), 0.90 – 0.66 (m, 16H).

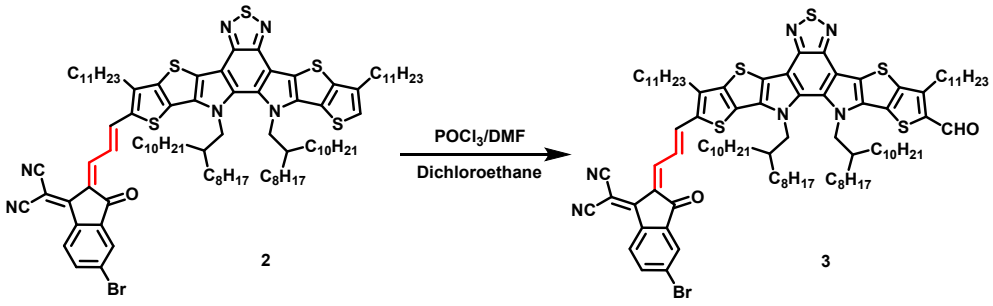


**Figure S4.** Synthesis of compound **3**.

Under argon protection, the flask was added with compound **2**(0.320 g 0.198 mmol), DMF(0.4 mL), dichloroethane(25 mL) and added $POCl_3$(0.4 mL) under ice water bath. After stirring for 1 hour, the reaction was carried out under the ice bath and starred at 60 ℃ for 6 hours. The reaction solution was poured into methanol and filtered. The compound **3** was obtained by column chromatography(PE:DCM=3:1). Dark green solid(0.280 g yield 86%). $^1$H NMR (500 MHz, Chloroform-d) δ 10.15 (s, 1H), 8.66 (dd, J = 14.3, 11.8 Hz, 1H), 8.57 – 8.51 (m, 2H), 8.00 (d, J = 1.9 Hz, 1H), 7.87 (dd, J = 8.4, 2.0 Hz, 1H), 7.73 (d, J = 14.3 Hz, 1H), 4.63 (d, J = 7.8 Hz, 4H), 3.20 (t, J = 7.8 Hz, 2H), 3.02 (t, J = 7.9 Hz, 2H), 2.06 (s, 2H), 1.89 (dq, J = 31.7, 7.8 Hz, 4H), 1.55 (s, 6H), 1.53 – 1.44 (m, 1H), 1.39 (s, 1H), 1.35 – 1.20 (m, 33H), 1.20 – 0.52 (m, 33H).

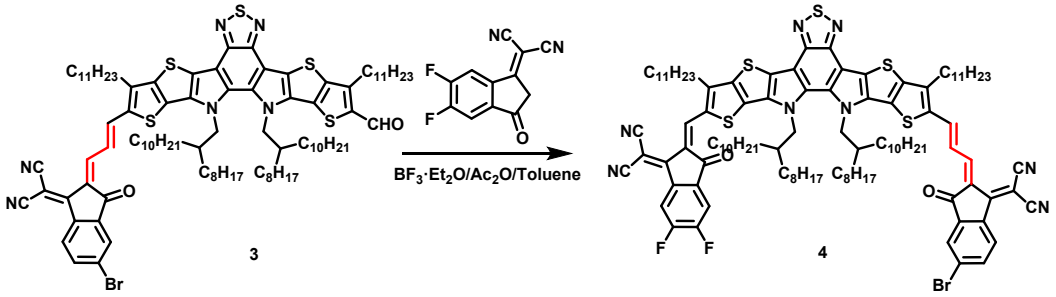


**Figure S5.** Synthesis of compound **4**.

To the flask was added compound **3**(0.213 g 0.130 mmol), 2F-IC(0.033 g 0.143mmol), $BF_3$·$Et_2O$(0.3 mL), $Ac_2O$(0.3 mL) and toluene(20 mL). After stirring for 10 mins, the reaction solution was poured into methanol and filtered. The compound **4** was obtained by column chromatography(PE:DCM=1.5:1). Dark solid(0.203 g yield 84%). $^1$H NMR (500 MHz, Chloroform-*d*) δ 9.17 (s, 1H), 8.68 (dd, *J* = 14.4, 11.7 Hz, 1H), 8.62 – 8.50 (m, 3H), 8.02 (d, *J* = 1.9 Hz, 1H), 7.88 (dd, *J* = 8.4, 2.0 Hz, 1H), 7.77 – 7.65 (m, 2H), 4.74 (d, *J* = 7.7 Hz, 2H), 4.66 (d, *J* = 7.9 Hz, 2H), 3.24 (t, *J* = 8.0 Hz, 2H), 3.03 (t, *J* = 7.9 Hz, 2H), 2.15 – 1.96 (m, 3H), 1.88 (h, *J* = 7.9 Hz, 4H), 1.55 (s, 13H), 1.44 – 1.17 (m, 44H), 1.20 – 0.91 (m, 52H), 0.92 – 0.68 (m, 23H).

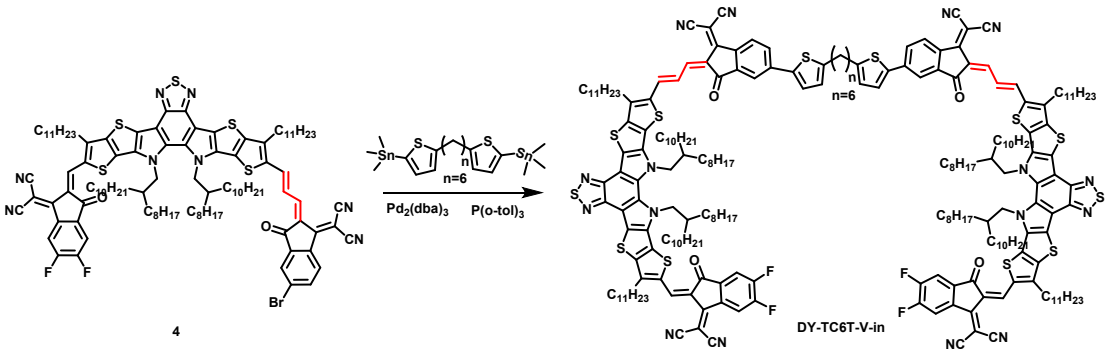


**Figure S6.** Synthesis of compound **DY-TC6T-V-in**.

Under argon protection, the flask was added with compound **4**(0.150 g 0.081 mmol), 1,6-Bis(5-(trimethylstannyl)thiophen-2-yl)hexane(0.021 g 0.037 mmol), $Pd_2(dba)_3$(1 mg), $P(o\text{-}tol)_3$(1.34 mg), toluene(15 mL) and stirred vigorously at 110 ℃ for 3 h. The reaction solution was poured into methanol and filtered. The compound **DY-TC6T-V-in** was obtained by column chromatography(PE:DCM=1:1). Dark solid(0.124 g yield 90%). $^1$H NMR (400 MHz, Chloroform-d) δ 9.16 (s, 2H), 8.75 – 8.63 (m, 4H), 8.60 – 8.47 (m, 4H), 8.01 (d, J = 1.9 Hz, 2H), 7.91 (dd, J = 8.4, 1.9 Hz, 2H), 7.71 – 7.66 (m, 4H), 7.42 (d, J = 3.6 Hz, 2H), 6.88 (d, J = 3.6 Hz, 2H), 4.74 (d, J = 7.7 Hz, 4H), 4.66 (d, J = 7.7 Hz, 4H), 3.24 (t, J = 7.9 Hz, 4H), 3.02 (t, J = 7.8 Hz, 4H), 2.91 (t, J = 7.5 Hz, 4H), 2.14 – 1.97 (m, 6H), 1.85 (dd, J = 23.7, 15.9 Hz, 12H), 1.57 (s, 35H), 1.26 (d, J = 5.0 Hz, 50H), 1.19 – 0.91 (m, 106H), 0.91 – 0.67 (m, 41H). $^{13}$C NMR (126 MHz, Chloroform-d) δ 149.48, 140.86, 139.32, 138.31, 137.89, 134.81, 131.19, 126.18, 126.04, 115.02, 55.65, 55.44, 39.08, 38.84, 31.92, 31.84, 31.79, 31.30, 30.62, 30.36, 30.12, 29.90, 29.82, 29.77, 29.74, 29.70, 29.67, 29.63, 29.58, 29.56, 29.54, 29.50, 29.46, 29.44, 29.42, 29.38, 29.35, 29.34, 29.21, 28.72, 28.65, 25.67, 25.48, 22.69, 22.62, 14.11, 14.10. HRMS (MALDI-FTICR-MS) m/z: [M]+ calcd. for $C_{230}H_{290}F_4N_{16}O_4S_{12}$:3801.9633;found [M]+: 3802.9666.

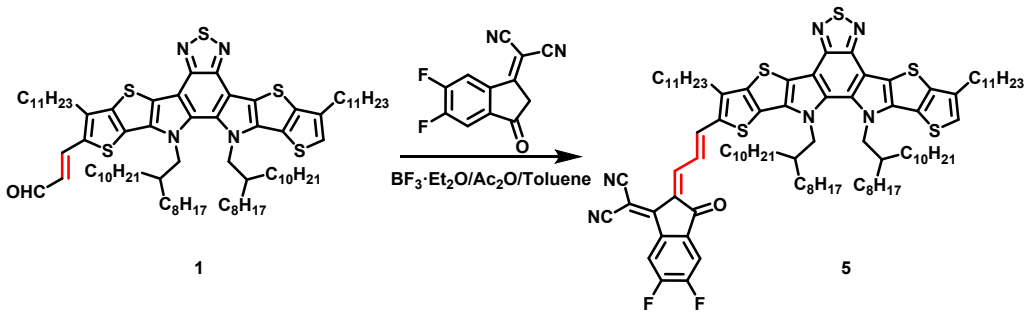


**Figure S7.** Synthesis of compound **5**.

To the flask was added compound **1**(0.543 g 0.399 mmol), 2F-IC(0.100 g 0.434 mmol), $BF_3{\cdot}Et_2O$(0.15 mL), $Ac_2O$(0.3 mL) and toluene(30 mL). After stirring for 10 mins, the reaction solution was poured into methanol and filtered. The compound **5** was obtained by column chromatography(PE:DCM=3:1). Dark green solid(0.400 g, yield 64%). $^1$H NMR (400 MHz, Chloroform-d) δ 8.62 (dd, J = 14.0, 11.8 Hz, 1H), 8.57 – 8.47 (m, 2H), 7.75 (d, J = 14.1 Hz, 1H), 7.65 (t, J = 7.5 Hz, 1H), 7.08 (d, J = 1.1 Hz, 1H), 4.61 (d, J = 7.7 Hz, 4H), 3.02 (t, J = 7.8 Hz, 2H), 2.83 (t, J = 7.8 Hz, 2H), 2.05 (dt, J = 14.2, 6.8 Hz, 1H), 1.86 (s, 4H), 1.67 – 1.36 (m, 20H), 1.36 – 1.11 (m, 46H), 1.01 (d, J = 36.4 Hz, 78H), 0.89 – 0.58 (m, 17H).

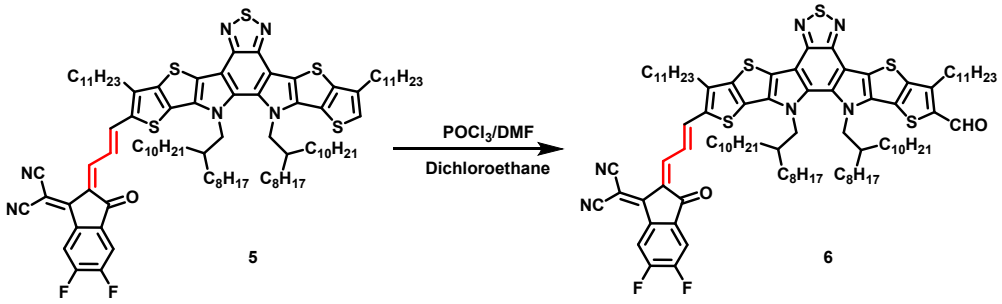


**Figure S8.** Synthesis of compound **6**.

Under argon protection, the flask was added with compound **5**(0.400 g 0.254 mmol), DMF(0.4 mL), dichloroethane(40 mL) and added $POCl_3$(0.4 mL) under ice water bath. After stirring for 1 hour, the reaction was carried out under the ice bath and starred at 60 ℃ for 6 hours. The reaction solution was poured into methanol and filtered. The compound **6** was obtained by column chromatography(PE:DCM=3:1). Dark green solid(0.360 g yield 88%). $^1$H NMR (400 MHz, Chloroform-d) δ 10.15 (s, 1H), 8.64 (dd, J = 14.3, 11.8 Hz, 1H), 8.59 – 8.47 (m, 2H), 7.74 (d, J = 14.2 Hz, 1H), 7.67 (t, J = 7.4 Hz, 1H), 4.67 – 4.56 (m, 4H), 3.20 (t, J = 7.8 Hz, 2H), 3.03 (t, J = 7.9 Hz, 2H), 2.04 (d, J = 13.9 Hz, 3H), 1.90 (dt, J = 25.4, 7.5 Hz, 4H), 1.57 (s, 26H), 1.36 – 1.10 (m, 45H), 1.00 (d, J = 39.1 Hz, 54H), 0.91 – 0.61 (m, 21H).

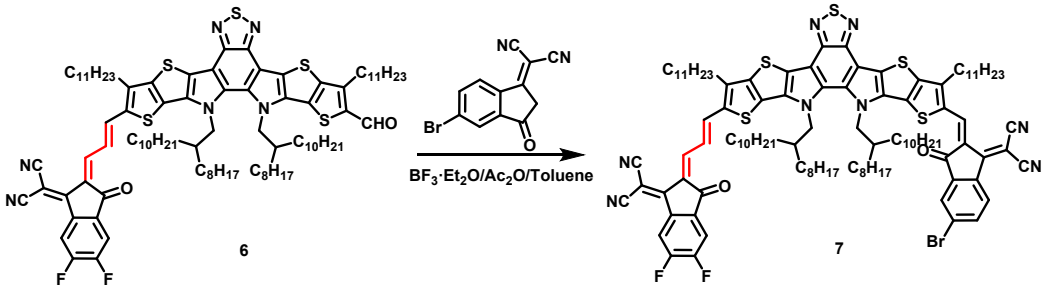


**Figure S9.** Synthesis of compound **7**.

To the flask was added compound **6**(0.360 g 0.225 mmol), Br-IC(0.068 g 0.247mmol), $BF_3$·$Et_2O$(0.4 mL), $Ac_2O$(0.4 mL) and toluene(30 mL). After stirring for 10 mins, the reaction solution was poured into methanol and filtered. The compound **7** was obtained by column chromatography(PE:DCM=1.5:1). Dark solid(0.334 g yield 80%). $^1$H NMR (400 MHz, Chloroform-d) δ 9.19 (s, 1H), 8.66 (dd, J = 14.3, 11.7 Hz, 1H), 8.61 – 8.48 (m, 3H), 8.04 (d, J = 2.0 Hz, 1H), 7.87 (dd, J = 8.4, 2.0 Hz, 1H), 7.77 – 7.66 (m, 2H), 4.74 (d, J = 7.7 Hz, 2H), 4.66 (d, J = 7.7 Hz, 2H), 3.24 (t, J = 7.9 Hz, 2H), 3.03 (t, J = 7.8 Hz, 2H), 2.10 (d, J = 8.1 Hz, 3H), 1.95 – 1.80 (m, 4H), 1.56 (s, 8H), 1.35 – 1.20 (m, 30H), 1.20 – 0.91 (m, 74H), 0.91 – 0.62 (m, 19H).

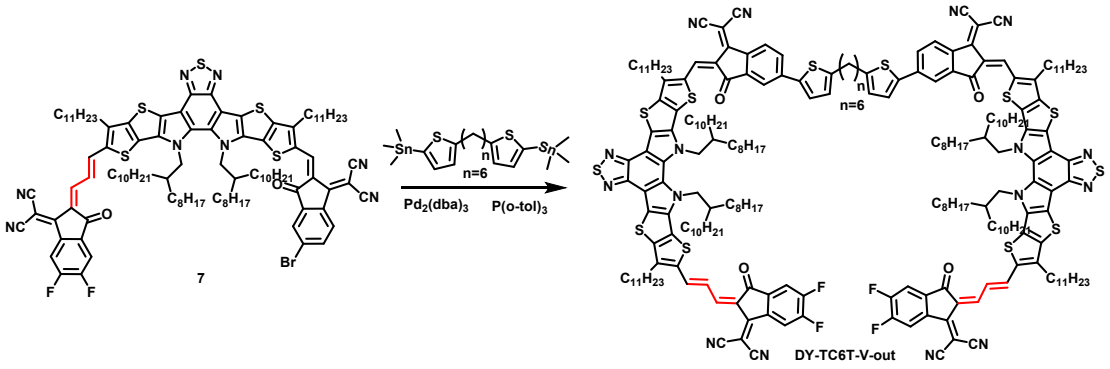


**Figure S10.** Synthesis of compound **DY-TC6T-V-out**.

Under argon protection, the flask was added with compound **7**(0.130 g 0.070 mmol), 1,6-Bis(5-(trimethylstannyl)thiophen-2-yl)hexane(0.018 g 0.031 mmol), $Pd_2(dba)_3$(0.88 mg), $P(o\text{-}tol)_3$(1.2 mg), toluene(10

mL) and stirred vigorously at 110 ℃ for 3 h. The reaction solution was poured into methanol and filtered. The compound **DY-TC6T-V-out** was obtained by column chromatography(PE:DCM=1:1). Dark solid(0.093 g yield 80%). $^1$H NMR (400 MHz, Chloroform-d) δ 9.14 (s, 2H), 8.72 – 8.58 (m, 4H), 8.57 – 8.46 (m, 4H), 8.02 (d, J = 1.9 Hz, 2H), 7.90 (dd, J = 8.3, 1.9 Hz, 2H), 7.73 (d, J = 14.1 Hz, 2H), 7.65 (t, J = 7.5 Hz, 2H), 7.40 (d, J = 3.6 Hz, 2H), 6.87 (d, J = 3.6 Hz, 2H), 4.76 (d, J = 7.7 Hz, 4H), 4.67 (d, J = 7.8 Hz, 4H), 3.18 (t, J = 8.0 Hz, 4H), 3.03 (t, J = 8.0 Hz, 4H), 2.91 (t, J = 7.4 Hz, 4H), 2.13 (s, 4H), 2.07 – 1.97 (m, 3H), 1.94 – 1.73 (m, 5H), 1.57 (s, 77H), 1.26 (d, J = 5.9 Hz, 90H), 1.06 (dd, J = 51.8, 7.9 Hz, 54H), 0.91 – 0.68 (m, 33H). $^{13}$C NMR (126 MHz, Chloroform-d) δ 149.28, 139.40, 137.98, 137.90, 131.04, 130.13, 128.09, 126.14, 125.85, 118.76, 39.01, 38.84, 31.94, 31.92, 31.90, 31.81, 31.27, 31.15, 30.60, 30.38, 30.22, 29.85, 29.82, 29.75, 29.68, 29.66, 29.63, 29.59, 29.57, 29.55, 29.47, 29.41, 29.34, 29.22, 29.20, 28.75, 25.66, 25.51, 22.69, 22.62, 14.11, 14.09. HRMS (MALDI-FTICR-MS) m/z: [M]+ calcd. for $C_{230}H_{290}F_4N_{16}O_4S_{12}$: 3801.9633, found [M]+: 3802.9666.

## 2. $^1$H, $^{13}$C NMR and Mass spectra.

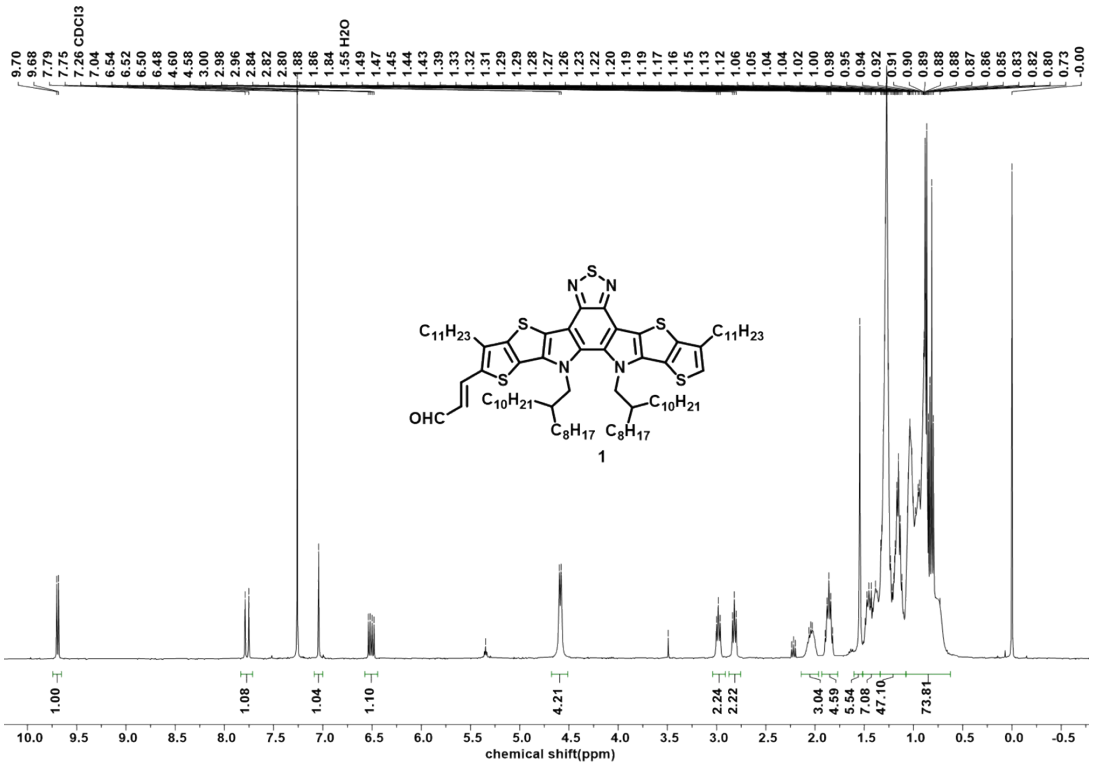


**Figure S11.** $^1$H NMR spectrum of compound **1** in $CDCl_3$.

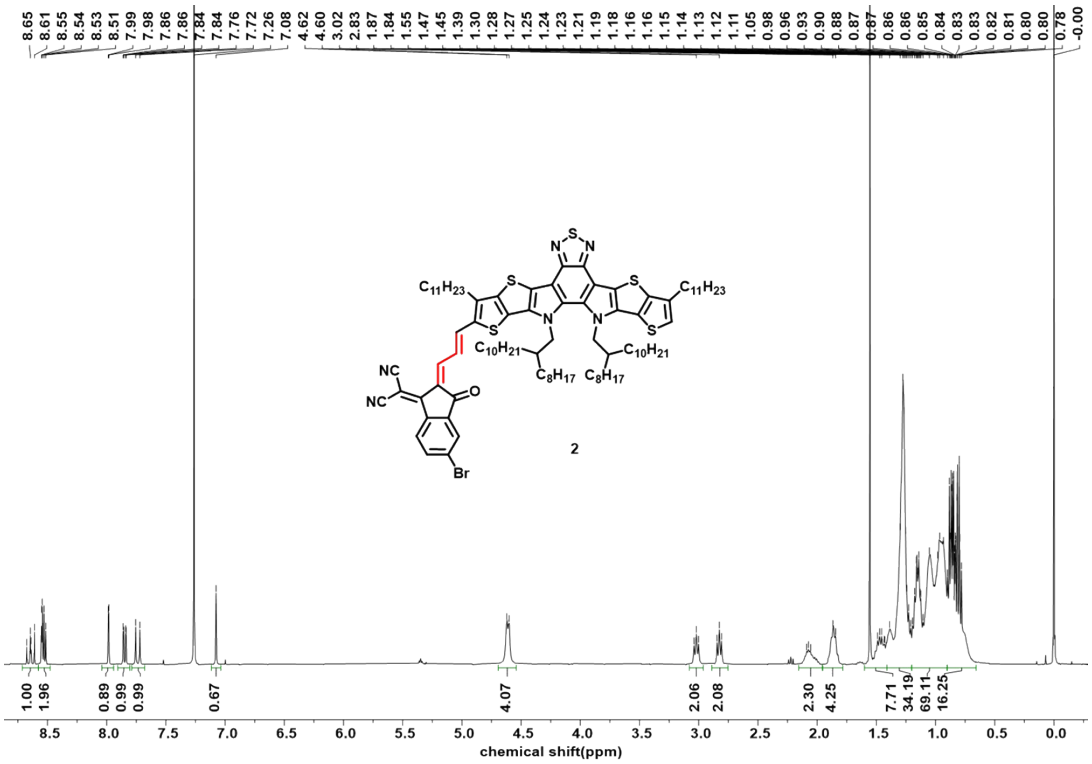


**Figure S12.** $^{1}$H NMR spectrum of compound **2** in $CDCl_3$.

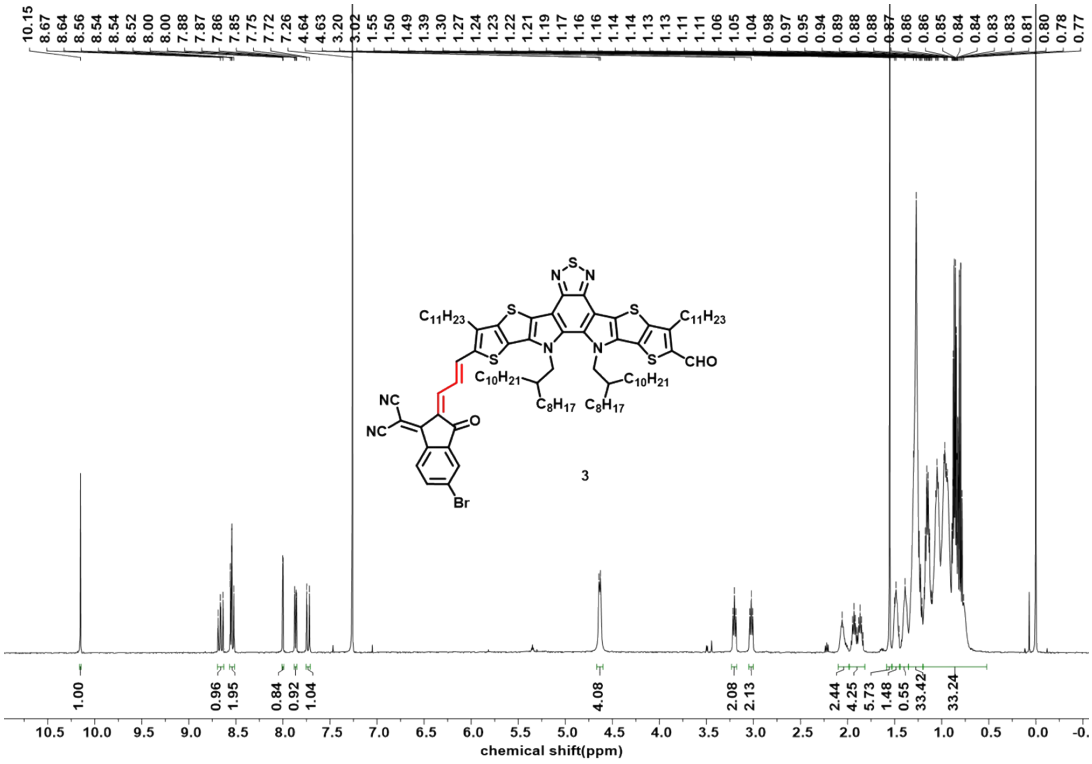


**Figure S13.** $^{1}$H NMR spectrum of compound **3** in $CDCl_3$.

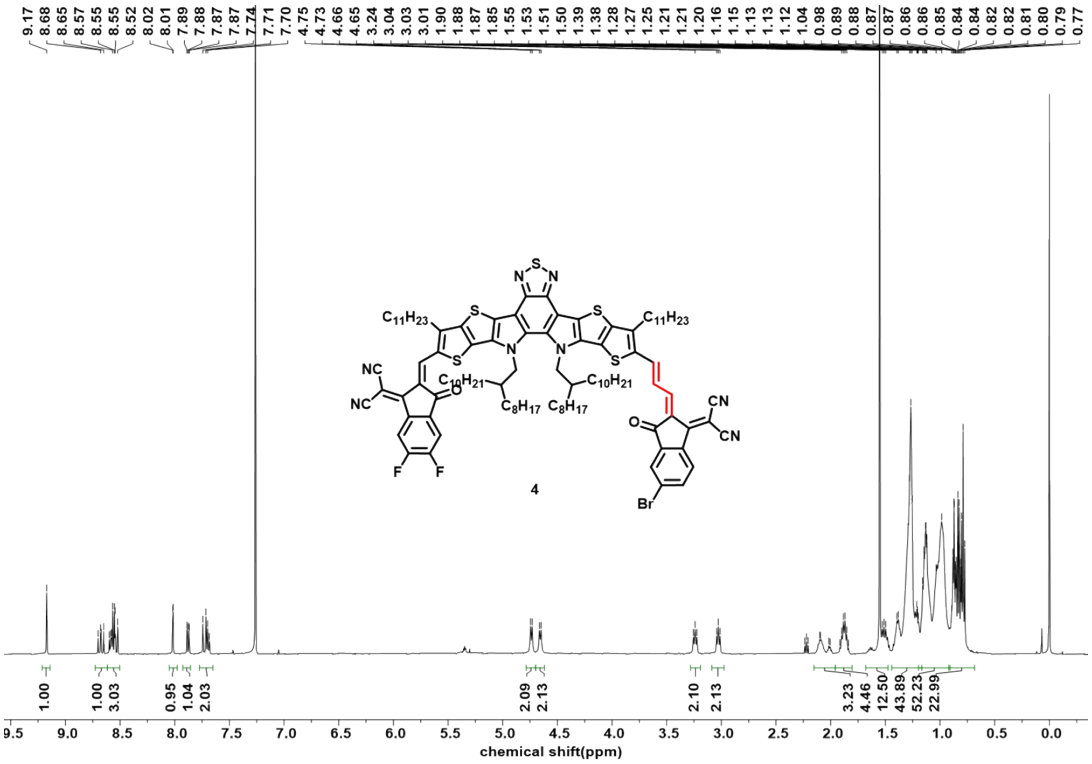


**Figure S14.** $^{1}$H NMR spectrum of compound **4** in $CDCl_3$.

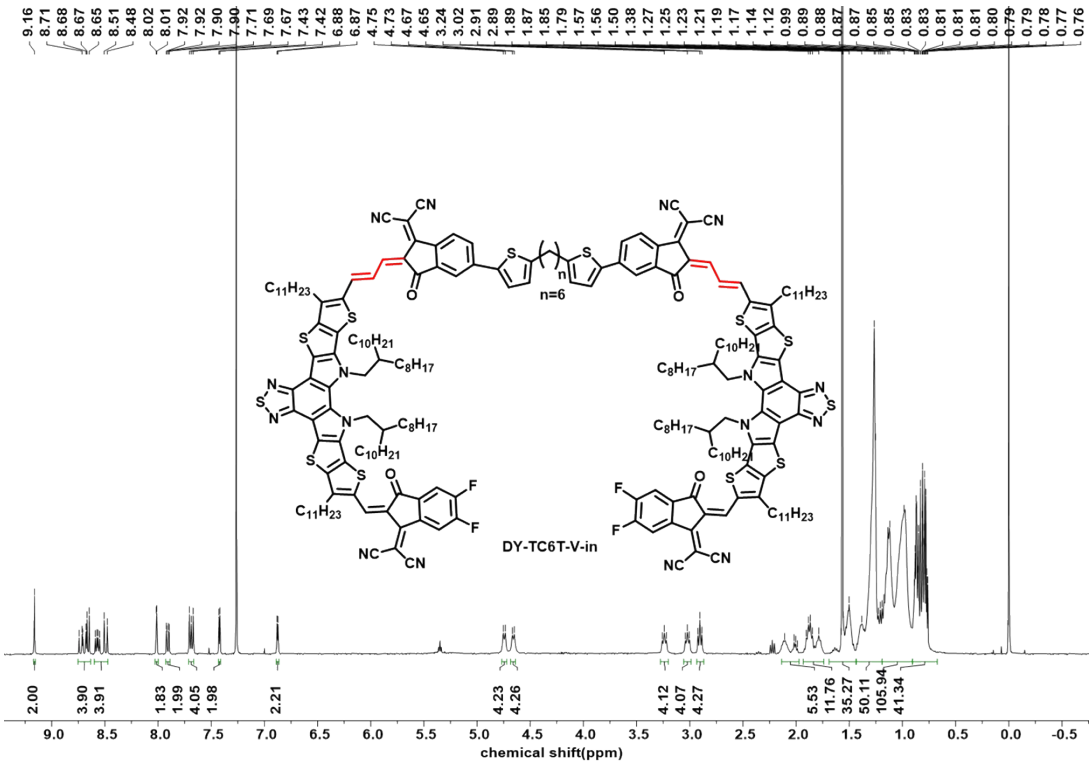


**Figure S15.** $^{1}$H NMR spectrum of compound **DY-TC6T-V-in** in $CDCl_3$.

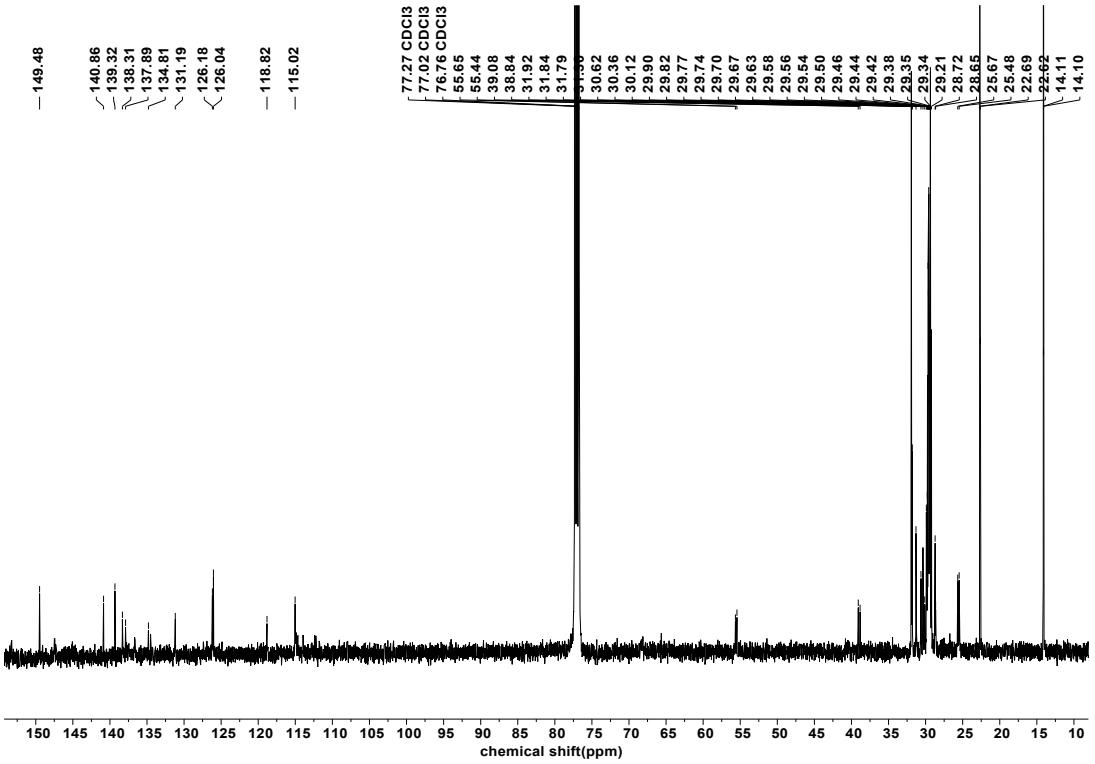


**Figure S16.** $^{13}C$ NMR spectrum of giant molecule **DY-TC6T-V-in** in $CDCl_3$.

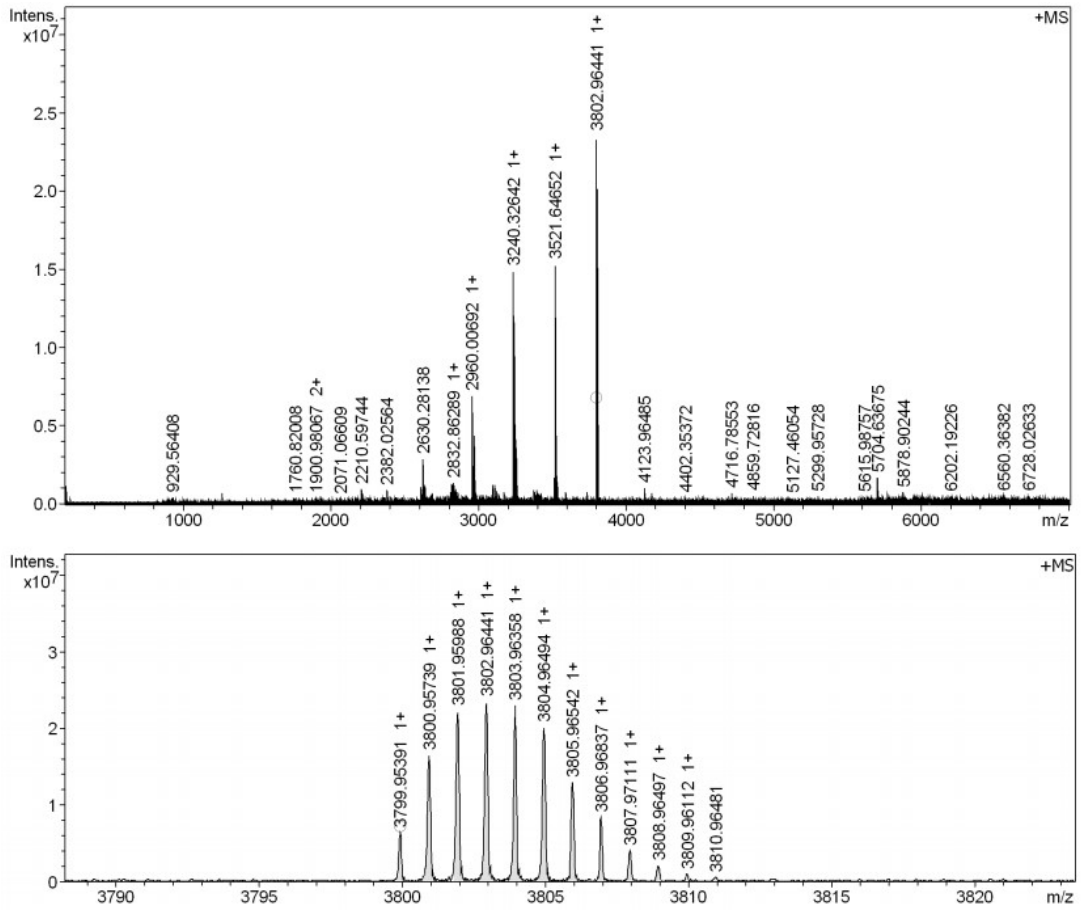


**Figure S17.** High resolution mass spectra of **DY-TC6T-V-in** .

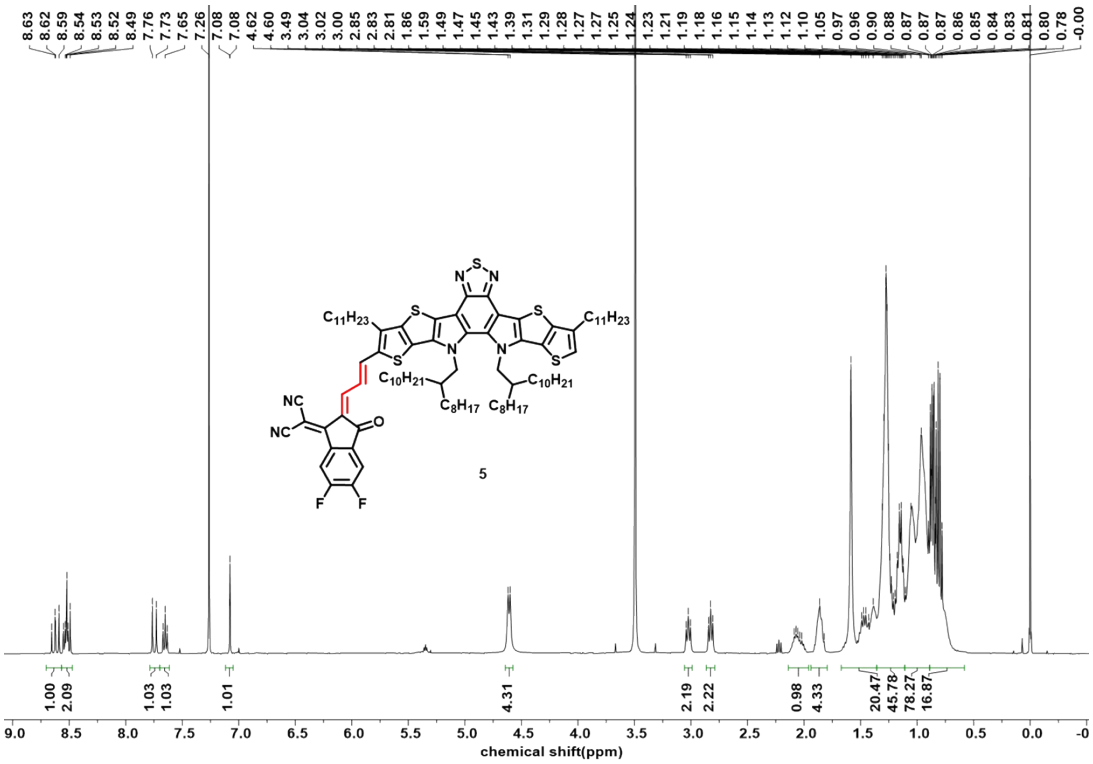


**Figure S18.** $^{1}H$ NMR spectrum of compound **5** in $CDCl_3$.

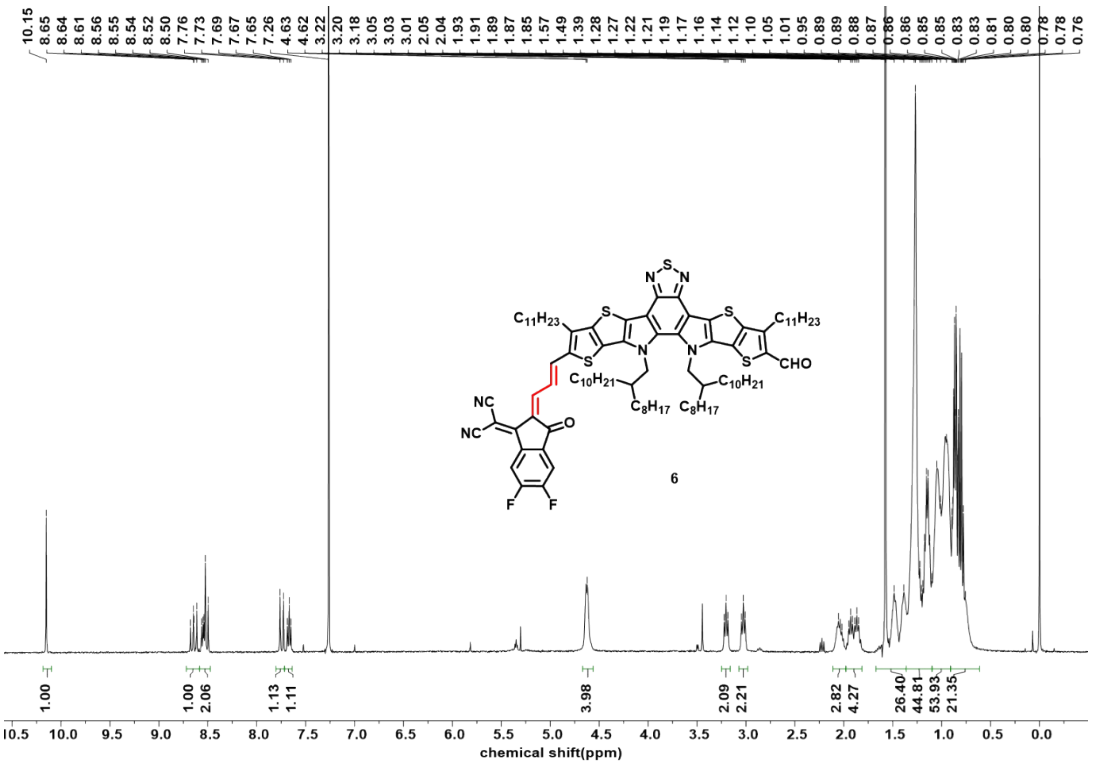


**Figure S19.** $^{1}H$ NMR spectrum of compound **6** in $CDCl_3$.

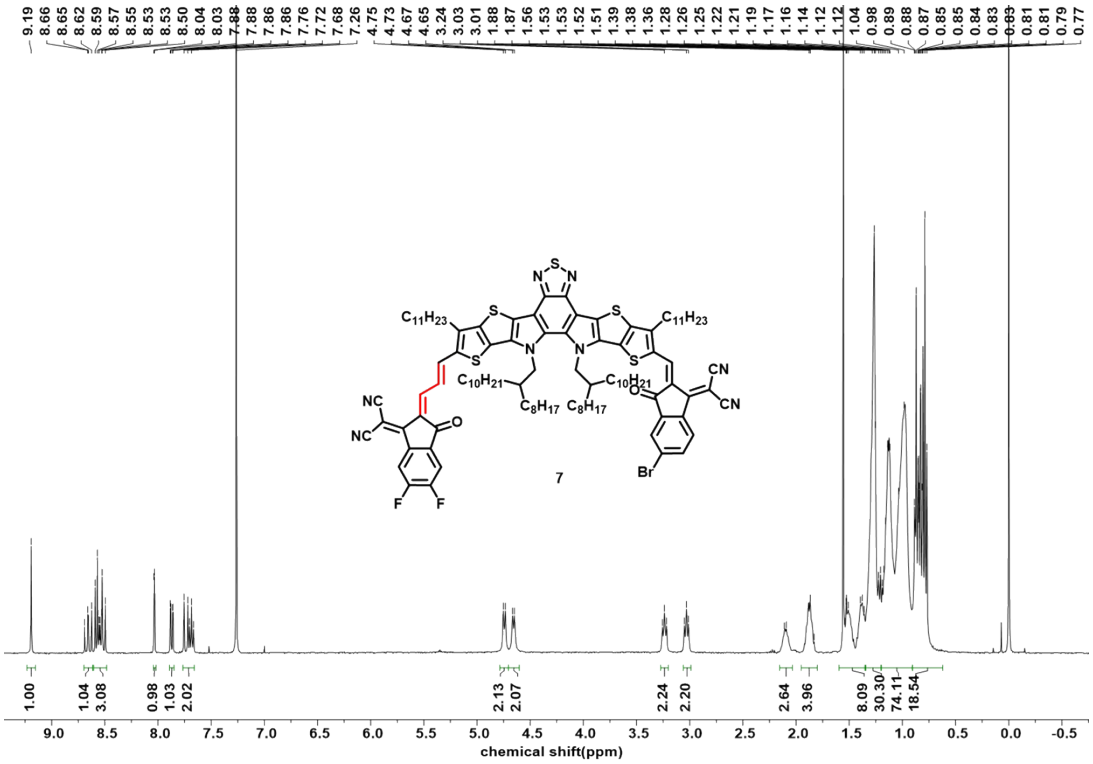


**Figure S20.** $^{1}$H spectrum of compound **7** in $CDCl_3$.

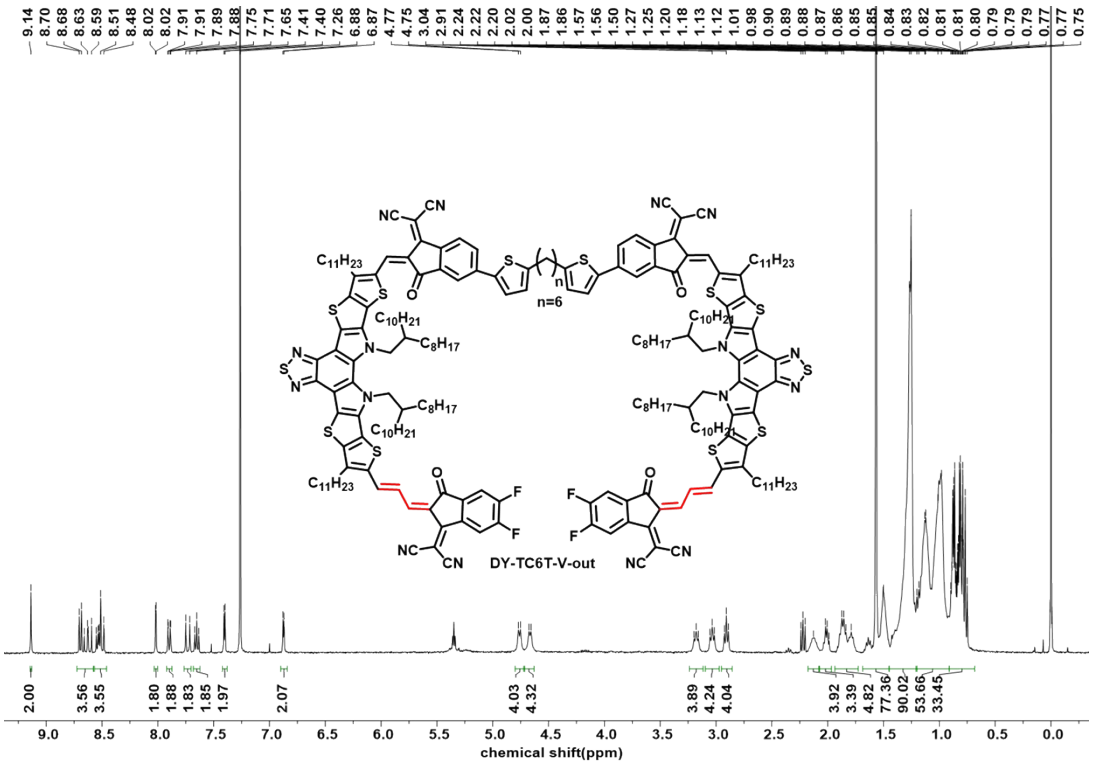


**Figure S21.** $^{1}$H spectrum of giant molecule **DY-TC6T-V-out** in $CDCl_3$.

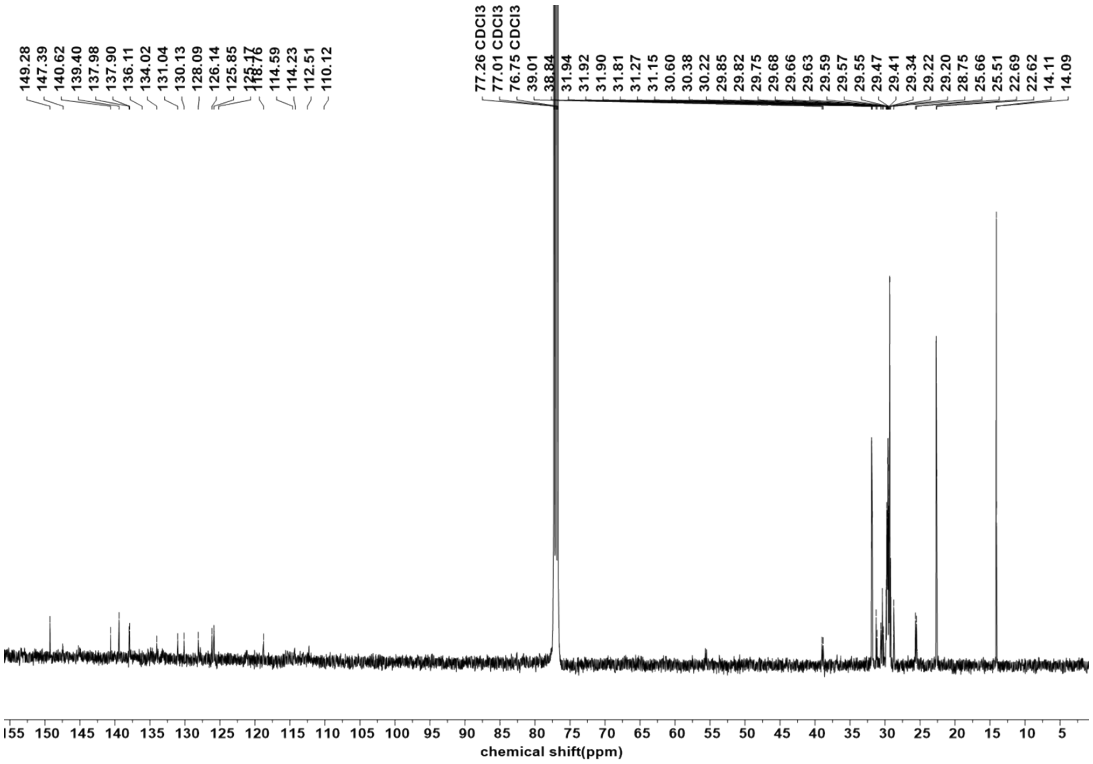


**Figure S22.** $^{13}C$ NMR spectrum of giant molecule **DY-TC6T-V-out** in $CDCl_3$.

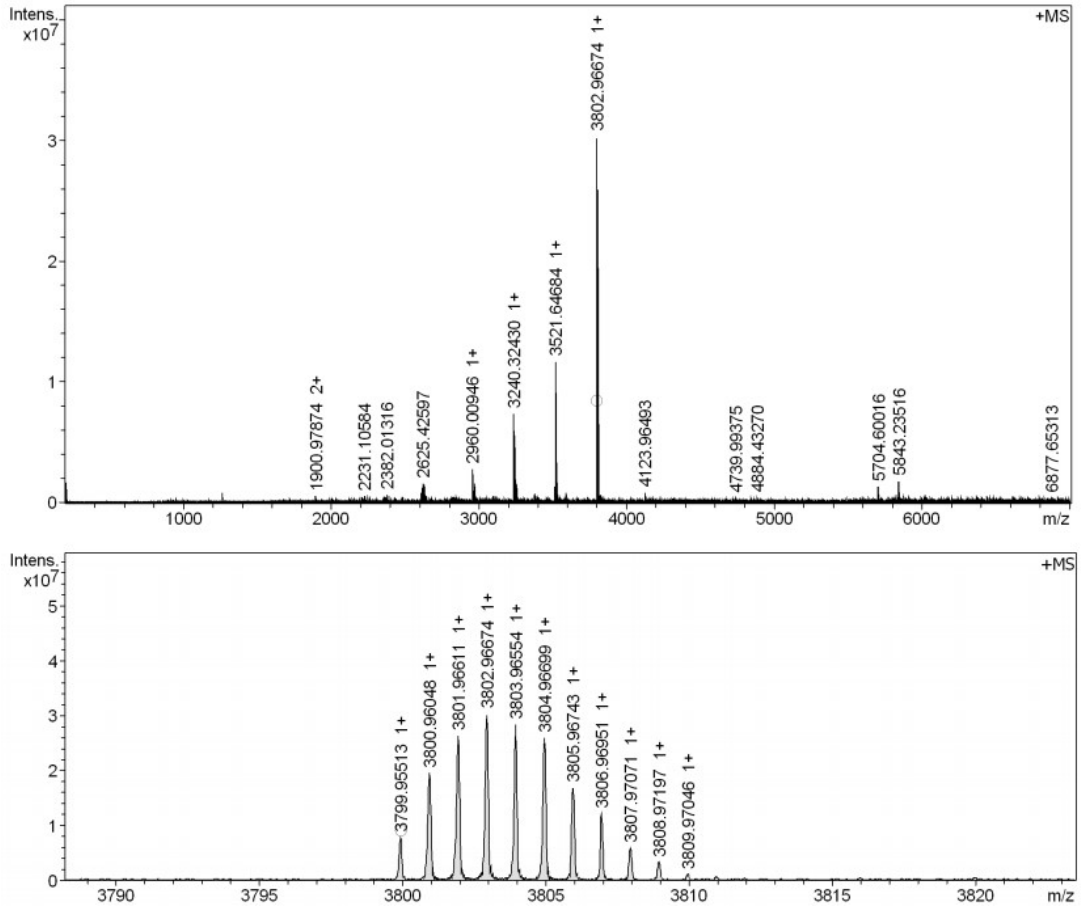


**Figure S23**. High resolution mass spectra of **DY-TC6T-V-out**.

## 3. Instruments and Measurements.

$^{1}$H NMR and $^{13}$C NMR spectra were recorded using a Bruker AV-400 spectrometer in a deuterated chloroform solution at 298 K, unless specified otherwise. Chemical shifts are reported as δ values (ppm) with tetramethylsilane (TMS) as the internal reference. The molecular mass was confirmed using an Autoflex III matrix-assisted laser desorption ionization mass spectrometer (MALDI-TOF MS). UV-Vis absorption spectra were recorded on the SHIMADZU UV-2600 spectrophotometer. The cyclic voltammetry results were obtained with a computer-controlled CHI 660E electrochemical workstation, the electrochemical properties of materials were tested by cyclic voltammetry (CV) at a scanning rate of 20 mV·s$^{-1}$. A three-electrode system was adopted, with ferrocene as the internal standard, glassy carbon electrode as the working electrode, Ag/AgCl electrode as the reference electrode, and Pt wire electrode as the counter electrode. The film of the material was coated on the glassy carbon electrode, and all electrodes were placed in an acetonitrile solution of 0.1mol/L tetrabutylammonium hexafluorophosphate for testing. The energy levels of the highest occupied molecular orbital (HOMO) and the lowest empty molecular orbital (LUMO) can be calculated by the following formula: $\mathrm{EHOMO/LUMO} = -(4.80 - E_{1/2,\,F_C/F_C^+} + E_{onset}^{ox/red})\ \mathrm{eV}$.

The glass transition temperature (Tg) of the materials was measured using ultraviolet-visible (UV-Vis) spectroscopy. films were thermally annealed within temperature ranges of 40–160°C, respectively. The absorption spectra of the films were tested at different annealing temperatures, with the film preparation conditions (i.e., solvent, concentration, and spin-coating speed) matching those used in organic solar cell fabrication. Glass transition temperature ($T_g$) of film samples was obtained by extracting the deviation metric (DM) from the temperature-dependent absorption spectra. Here, DM can be calculated based on the equation described as: $DM_T=\Sigma\lambda_{max}\lambda_{min}(I_{RT}(\lambda)-I_T(\lambda))^2$, where $I_{RT}(\lambda)$ and $I_T(\lambda)$ represent the absorption intensity of as-cast and annealed acceptor films, respectively.

Density Functional Theory (DFT) Calculations. Calculation level B3LYP/6-32G (d) was chosen for structural optimisation, electrostatic potential and electrostatic potential area distribution are viewed with Multiwfn.[3-5]

The morphologies of the blend films were investigated by atomic force microscopy (AFM, Agilent Technologies, 5500 AFM/SPM System, USA) in contacting mode with a 2 μm scanner.

Grazing Incidence Wide-Angle X-ray Scattering (GIWAXS) measurements were accomplished with a Xeuss 2.0 SAXS/WAXS laboratory beamline using a Cu X-ray source (8.05 keV, 1.54 Å) and a Pilatus3R 300K detector. The incidence angle is 0.2º. GIWAXS samples are prepared on silicon substrate by spin coating.

The transient absorption spectrometer (TAS) utilized in this study was a femtosecond system. A femtosecond laser amplifier (Solstice, Spectra-Physics) generated an 800 nm pulse at a frequency of 1 kHz, which was then split into two beams to produce the pump and probe pulses, respectively. The probe pulses were focused onto a 3 mm sapphire crystal and 8 mm YAG to generate visible light (450–790 nm) and infrared light (850-1500 nm). To control the time delay between the pump and probe pulses, a mechanical delay stage was employed. The pump pulse was modulated by a mechanical chopper operating at 500 Hz and then focus on the fixed sample together with probe beams. The probe beam was collected into a fiber-coupled spectrometer. The energy of the pump pulse was measured using a power meter (PM400, Thorlabs). And the beam size of the pump pulse was measured using a Beam profiler (BC106N-VIS/M, Thorlabs).

Contact angles were measured with a contact angle meter. The solution of each organic material was spin-coated on cleaned ITO substrates. Droplets of water and ethylene glycol were dripped onto the different films. According to Owens-Wendt method, surface energy could be divided into dispersive and polar components: $\gamma = \gamma d + \gamma p$.Furthermore, the dispersive and polar surface energy can be calculated though the formula below based on the contact angles obtained by two solvents: $(1+cos\theta)\,\gamma_l = \frac{4\gamma_l^d\gamma_s^d}{\gamma_l^d+\gamma_s^d} + \frac{4\gamma_l^p\gamma_s^p}{\gamma_l^p+\gamma_s^p}$, where $\theta$ is the contact angle

of a specific solvent, $\gamma_l$ is the surface energy of the solvent, $\gamma_s^d$ and $\gamma_s^p$ refer to the dispersive and polar surface energy of the solid, respectively, and $\gamma_l^d$ and $\gamma_l^p$ refer to the dispersive and polar surface energy of the solvent, respectively. Thus, the unknown value $\gamma_s^d$ and $\gamma_s^p$ can be solved through combining two equations obtained by contact angle measurement of two different solvents. The Flory–Huggins interaction parameter can be written as the formula below: $\chi_{ij} = \kappa(\sqrt{\gamma_i} - \sqrt{\gamma_j})^2$, where K is a positive constant, $\gamma_i$ and $\gamma_j$ are the surface energy of material i and j, respectively. γ is an important index to judge the molecular interaction and compatibility of the two materials. The smaller the χ-value is, the better miscibility is.

For light stability, the prepared batteries are placed under a solar simulation lamp and the testing duration is set. During this period, the performance degradation of the batteries is observed. In the film thermal stability test, the film thermal stability test sample is placed in an inert gas environment and is subjected to continuous thermal stress of 65°C by a heating plate.

## 4. Device fabrication and characterization.

The optimized solar cell devices were fabricated with a conventional structure of Glass/ITO/Ph-4PACZ (40 nm)/active layer/PDINOH (5 nm)/Ag. Pre-patterned indium tin oxide (ITO) coated glass substrates were cleaned sequentially with deionized water and isopropyl alcohol in an ultrasonic bath for 15 mins each. After blow-drying with high-purity nitrogen, the ITO substrates were treated in an ultraviolet-ozone (UV-Ozone) cleaning system for 25 mins. Subsequently, a thin layer of Ph-4PACZ(Ethanol without water as the solvent) was deposited onto the cleaned ITO substrates by spin-coating at 3000 rpm for 30 seconds, followed by annealing at 100 °C for 10 mins in a nitrogen-filled glovebox. Next, the photovoltaic active layers were spin-coated inside the glovebox from a chloroform (CF) solution. The solution contained PM6 and the acceptor with a total concentration of 15.4 mg/mL (weight ratio of 1:1.2), incorporating 10 mg/mL of DCBB as the additive. The optimal active layers were obtained by spin-coating at approximately 3500 rpm for 30 seconds. Then, a PDIN-OH layer was deposited on top of the active layer at 3000 rpm for 40 seconds. Finally, a 100 nm thick silver (Ag) top electrode was thermally evaporated through a shadow mask onto the cathode buffer layer under a vacuum pressure of $1.0\times10^{-4}$mbar.

The current density-voltage (J-V) curve was tested at room temperature using a Keithley 2400 source meter and AM 1.5G illumination (100 mW $cm^{-2}$) in a glove box. The solar simulator was the SS-F5 from Enlitech. The light intensity was calibrated using a silicon photodiode with a national renewable energy laboratory-certified KG2 filter. The effective area of the device was 4.84 $mm^2$. The external quantum efficiency (EQE) test was conducted using a commercial EQE testing system (QE-R3011, Enlitech), with a calibrated silicon detector (RC-S103011-E, Enlitech) used as a reference.

Electron mobility and hole mobility measurements. The electron mobility device adopted the ITO/ZnO/active layer/PDINN/Ag structure, and the hole mobility device adopted the ITO/PEDOT: PSS/Active layer/MoO3/Ag structure. The electron and hole mobilities were calculated according to the space charge limited current (SCLC) method by the equation: $J = 9\mu\varepsilon_r\varepsilon_0V^2/8d^3$, where J is the current density, μ is the electron or hole mobility, V is the internal voltage in the device, $\varepsilon_r$ is the relative dielectric constant of active layer material, $\varepsilon_0$ is the permittivity of empty space, and d is the thickness of the active layer, the membrane thickness was measured using the Surfcorder ET 200 probe-type profilometer.

Using the supporting software provided by Taiwan-based Guangyan, different simulated light intensities were set. The standard silicon cells were then calibrated. Subsequently, the J-V characteristics curves of the battery under this series of light intensities were tested, thereby obtaining the dependence of the short-circuit current

density and open-circuit voltage on the light intensity respectively.

Under the dark state, different voltages are applied using the Keithley 2400 digital source meter to test the J-V curves of the battery under various applied voltages. This allows the dark current of the battery to be obtained. Under a solar standard light intensity, different voltages are applied using the Keithley 2400 digital source meter to test the J-V curves of the battery under various applied voltages. This enables the photocurrent of the battery to be obtained. The test voltage range is -3 V to 3 V, with a step size of 0.02 V, and the sweep speed is set to 0.2 V/s.

## 5. Additional Figures and Tables.

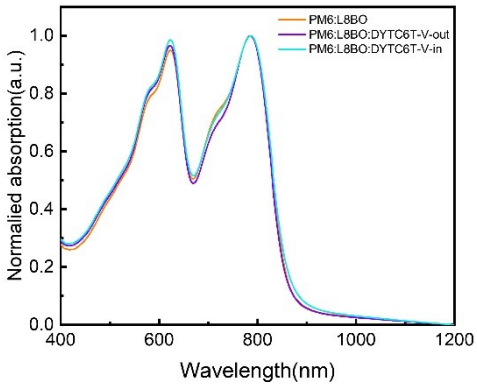


**Figure S24.** Absorption spectra of PM6:L8-BO, PM6:L8-BO:DYTC6T-V-out and PM6:L8-BO:DYTC6T-V-in.

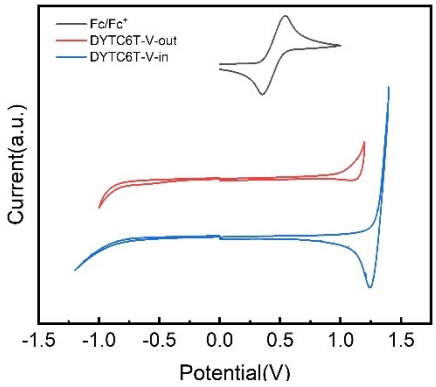


**Figure S25.** Cyclic voltammetry curves of DYTC6T-V-out and DYTC6T-V-in.

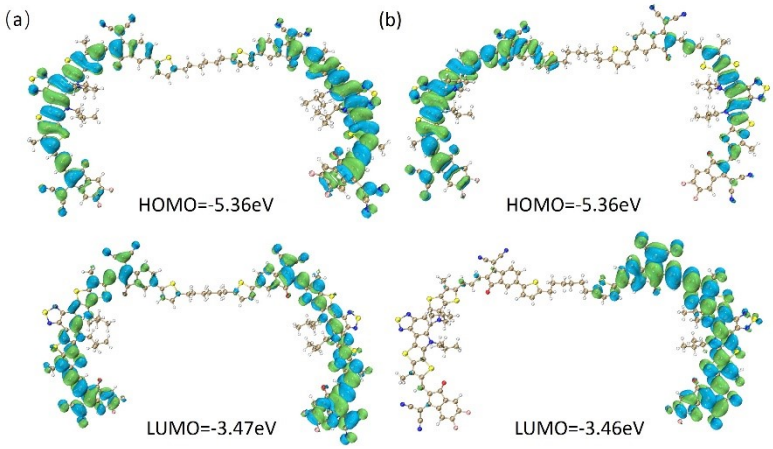

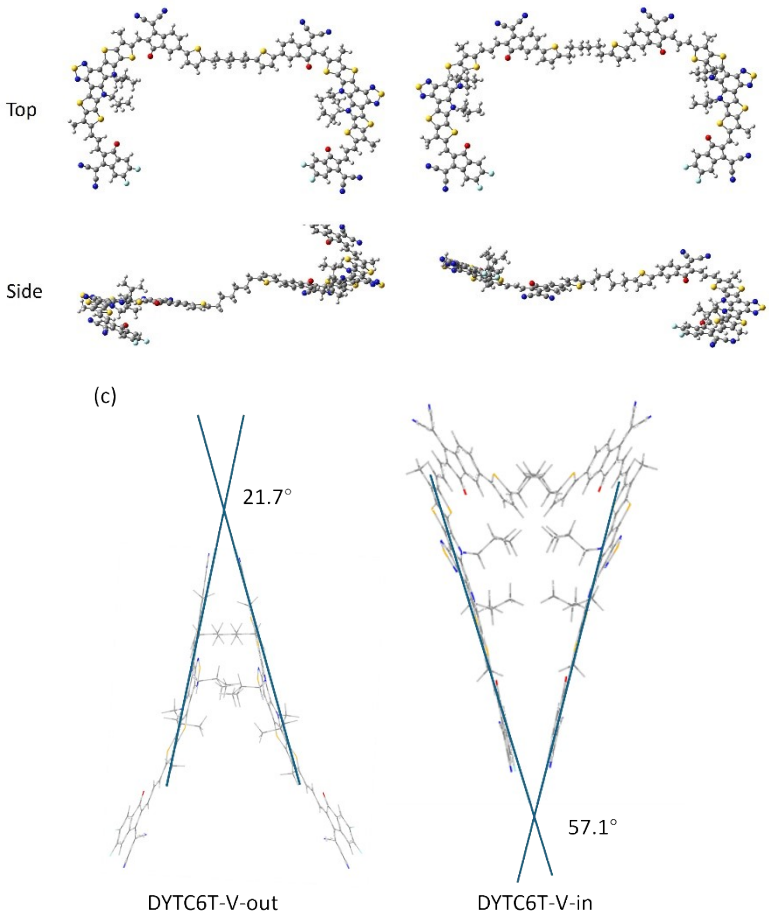


**Figure S26.** The simulated molecular geometries by DFT calculations for simplified molecules of the (a)DYTC6T-V-out and (b)DYTC6T-V-in from the top view and side view, and HUMO and LUMO energy levels, (c) The dihedral angle between the two small subunits of DYTC6T-V-out and DYTC6T-V-in.

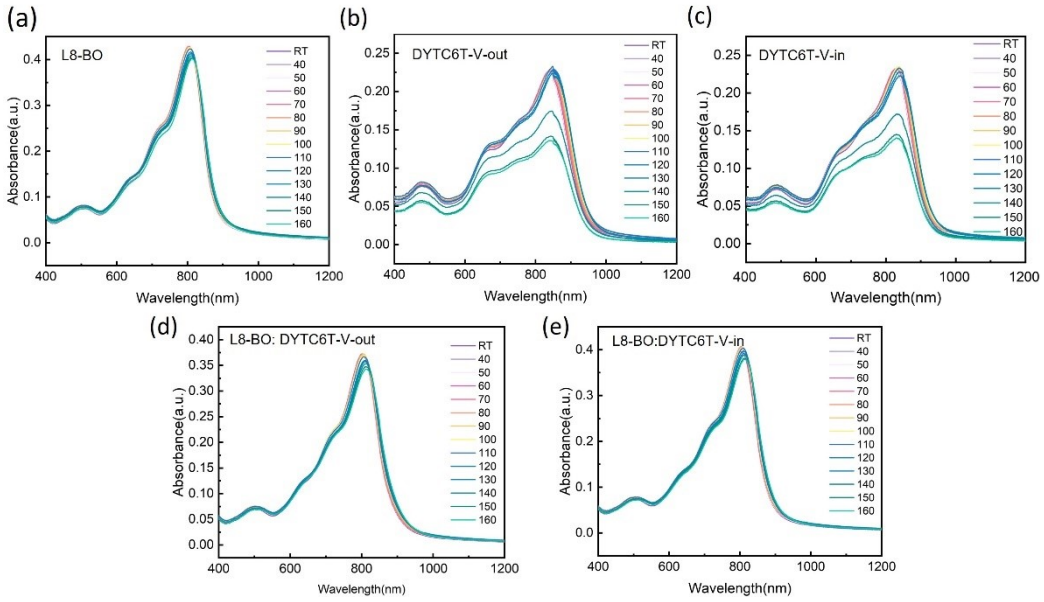


**Figure S27.** (a) Temperature-dependent absorption in solution of L8-BO, (b) DYTC6T-V-out, (c) DYTC6T-V-in, (d)L8-BO:DYTC6T-V-out and (e)L8-BO:DYTC6T-V-in.

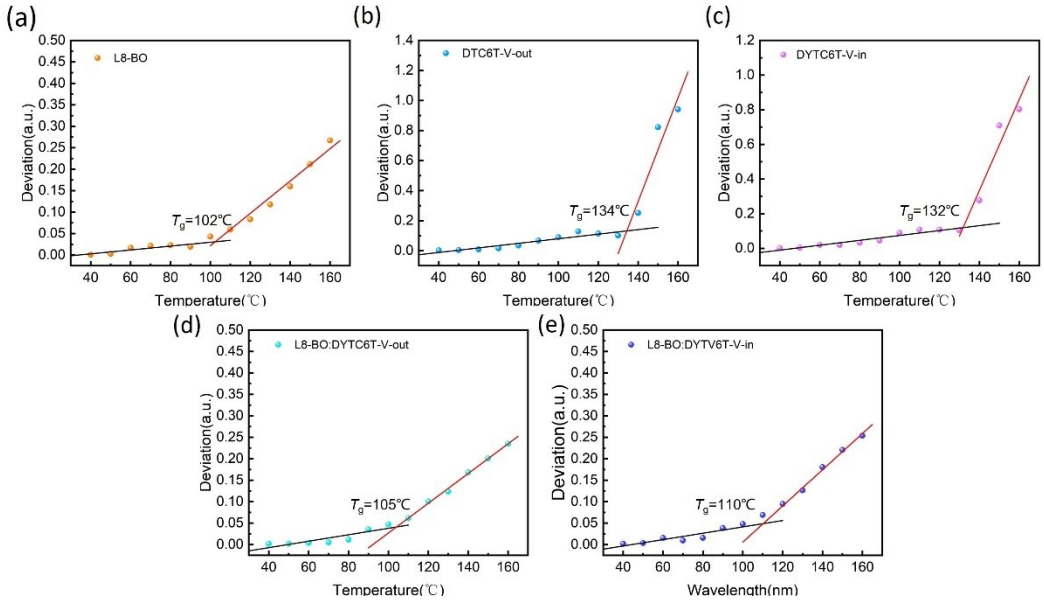


**Figure S28.** The measurements of $T_g$ values of (a)L8-BO, (b) DYTC6T-V-out, (c) DYTC6T-V-in, (d)L8-BO:DYTC6T-V-out and (e)L8-BO:DYTC6T-V-in. by fitting UV–vis deviation metric results.

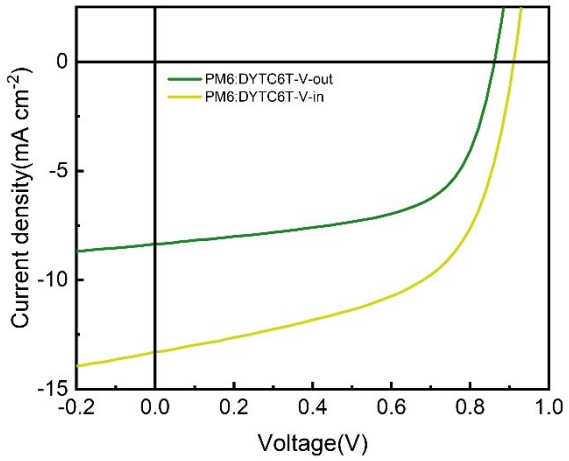


**Figure S29.** J–V curves of PM6:L8-BO:DYTC6T-V-out and PM6:L8-BO:DYTC6T-V-in.

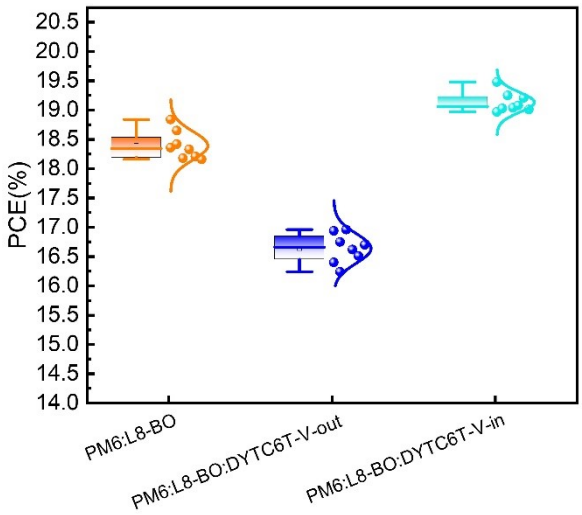


**Figure S30.** PCEs were obtained from 8 independent cells.

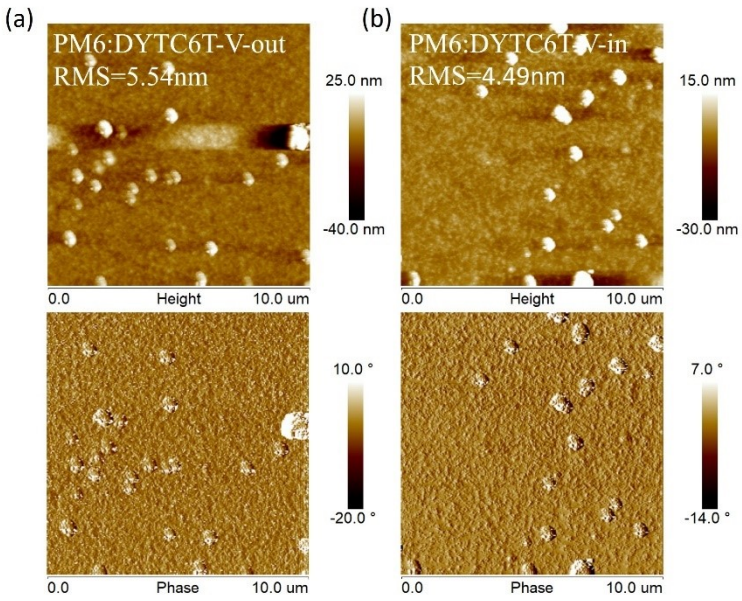


**Figure S31.** (a) AFM image of PM6:DYTC6T-V-out. (b) AFM image of PM6:DYTC6T-V-in.

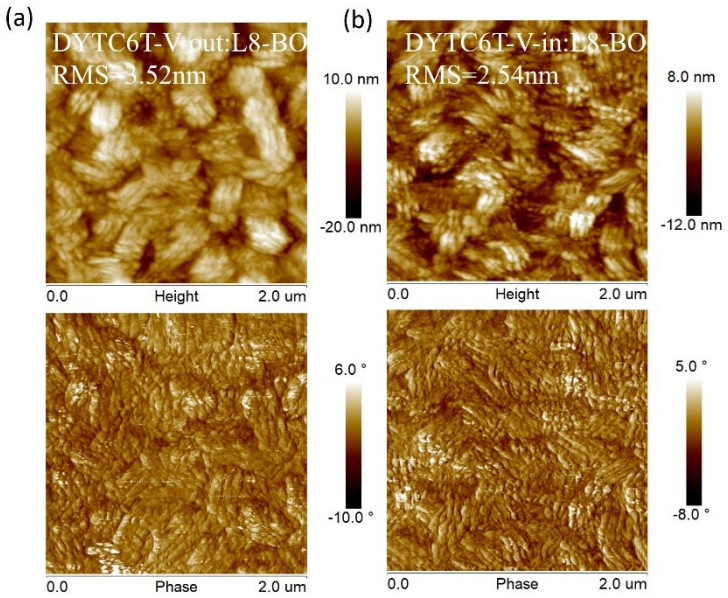


**Figure S32.** (a) AFM image of L8-BO:DYTC6T-V-out. (b) AFM image of L8-BO:DYTC6T-V-in.

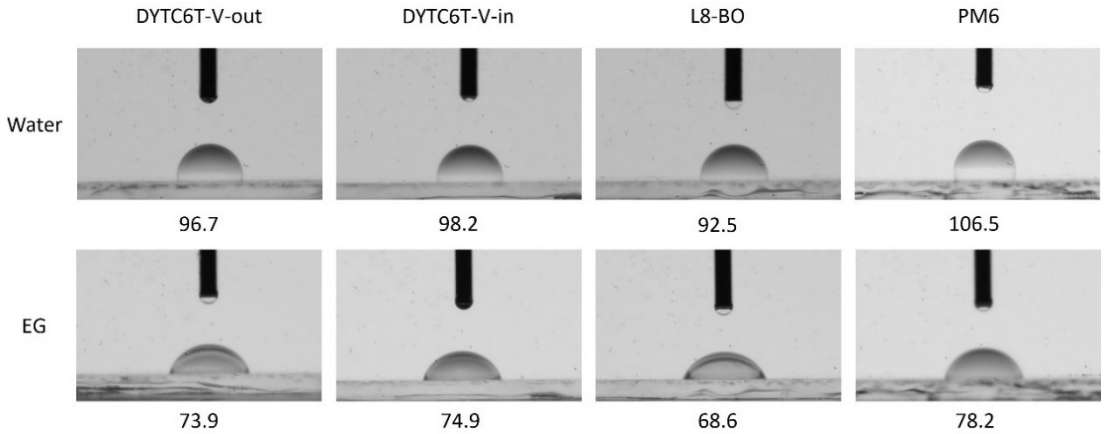


**Figure S33.** Contact angle images of water and ethylene glycol droplets on the neat films of PM6, DYTC6T-V-out, DYTC6T-V-in and L8-BO.

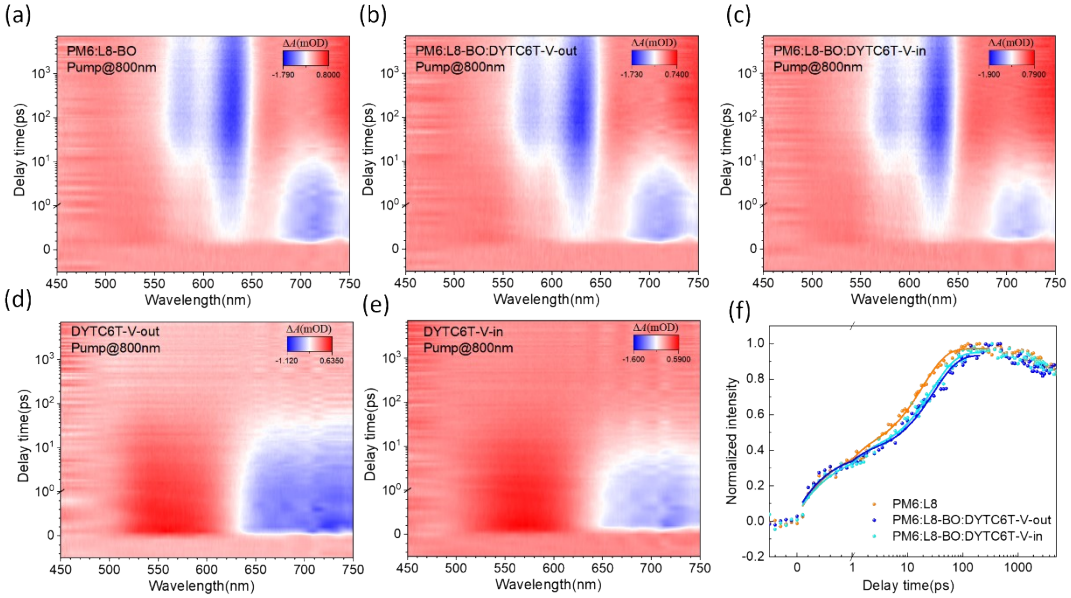


**Figure S34.** 2D TA spectra images of (a) PM6:L8-BO, (b) PM6:L8-BO:DYTC6T-V-out, (c) PM6:L8-BO:DYTC6T-V-in, (d)DYTC6T-V-out and (e)DYTC6T-V-in and (f) Normalized TAS spectra dynamic curves probed at 625–635 nm.

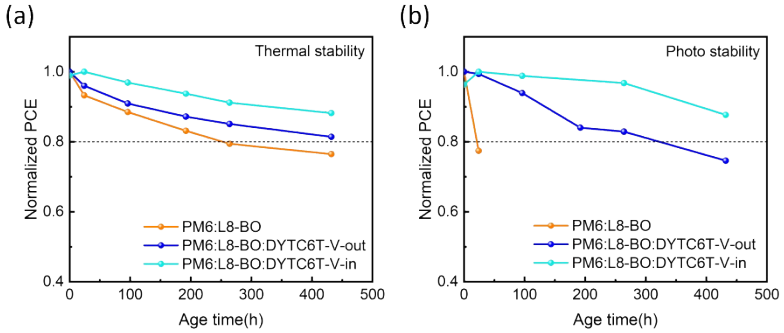


**Figure S35.** Thermal stability and photo stability of PM6:L8-BO, PM6:L8-BO:DYTC6T-V-out and PM6:L8-BO:DYTC6T-V-in in a glovebox under nitrogen without encapsulation.

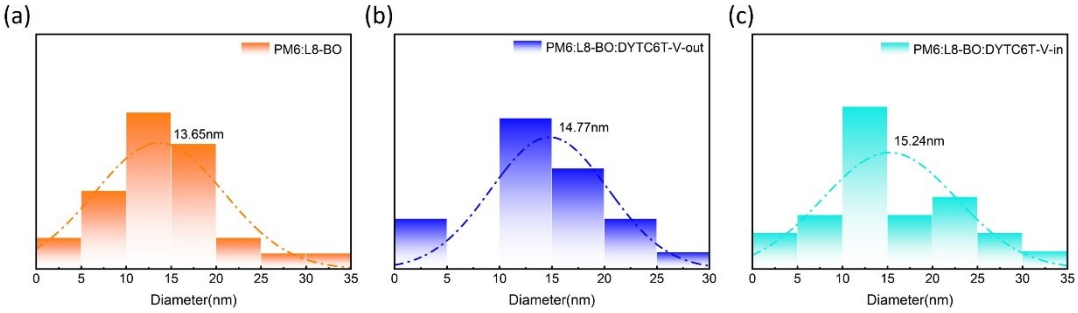


**Figure S36.** Fibril diameter distributions of blended films based on PM6:L8-BO, PM6:L8-BO:DYTC6T-V-out and PM6:L8-BO:DYTC6T-V-in.

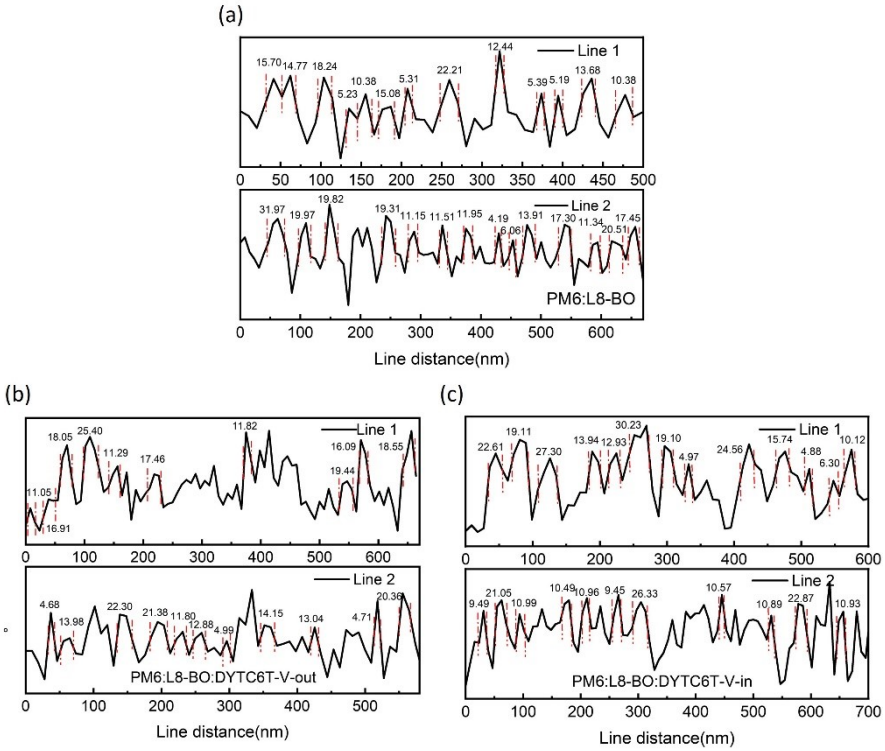


**Figure S37.** Line profiles across the AFM phase images of PM6:L8-BO, PM6:L8-BO:DYTC6T-V-out and PM6:L8-BO:DYTC6T-V-in.

**Table S1.** Device parameters of PM6:DYTC6T-V-out and PM6:DYTC6T-V-in

| D/A | active materials | $V_{oc}$(V) | FF(%) | $J_{sc}$(mA cm$^{-2}$) | PCE (%) |
|---|---|---|---|---|---|
| 1:1.2 | PM6:DYTC6T-V-out | 0.86 | 61.00 | 8.35 | 4.39 |
| 1:1.2 | PM6:DYTC6T-V-in | 0.91 | 56.44 | 13.30 | 6.83 |

**Table S2.** Contact angle and statistical data of surface tension and interaction parameter

| Materials | Water | EG | γd/(mN m$^{-1}$) | γp/(mN m$^{-1}$) | γ/(mN m$^{-1}$) | χ/K(γD$^{-2}$-γA$^{-2}$)$^2$ | χ/K(γA1$^{-2}$-γA2$^{-2}$)$^2$ |
|---|---|---|---|---|---|---|---|
| PM6 | 106.5 | 78.2 | 31.41 | 0.05 | 31.46 | / | / |
| L8-BO | 92.5 | 68.6 | 14.07 | 10.65 | 24.72 | 0.405 | / |
| DYTC6T-V-out | 96.7 | 73.9 | 13.19 | 9.23 | 22.42 | 0.767 | 0.056 |
| DYTC6T-V-in | 98.2 | 74.9 | 13.94 | 8.18 | 22.13 | 0.818 | 0.072 |

**Table S3.** GIWAXS parameters of the blend films.

| | in plane | | | out of plane | | |
|---|---|---|---|---|---|---|
| | location(Å$^{-1}$) | d-spacing(Å) | CCL(Å) | location(Å$^{-1}$) | d-spacing(Å) | CCL(Å) |
| PM6:L8-BO | 0.311 | 20.20 | 54.37 | 1.796 | 3.50 | 27.06 |
| PM6:L8-BO:DYTC6T-V-out | 0.317 | 19.82 | 47.12 | 1.768 | 3.55 | 27.19 |
| PM6:L8-BO:DYTC6T-V-in | 0.315 | 19.95 | 60.16 | 1.757 | 3.58 | 31.59 |

**Table S4.** The detailed biexponential function estimate result of HT kinetics.

| | A1 | $\tau_1$(ps) | A2 | $\tau_2$(ps) |
|---|---|---|---|---|
| PM6:L8-BO | 0.36 | 0.60 | 0.59 | 18.60 |
| PM6:L8-BO:DYTC6T-V-out | 0.32 | 0.54 | 0.56 | 29.80 |
| PM6:L8-BO:DYTC6T-V-in | 0.34 | 0.67 | 0.57 | 28.1 |


1. Z. Jia, X. Guo, X. Yin, M. Sun, J. Qiao, X. Jiang, X. Wang, Y. Wang, Z. Dong, Z. Shi, C.-H. Kuan, J. Hu, Q. Zhou, X. Jia, J. Chen, Z. Wei, S. Liu, H. Liang, N. Li, L. K. Lee, R. Guo, S. V. Roth, P. Müller-Buschbaum, X. Hao, X. Du and Y. Hou, *Nature*, 2025, **643**, 104-110.
2. Y. Zhou, Y. Zhong, S. Yuan, H. Cheng, W. Li, J. Han, J. Zhang, K. Han, J. Yuan, Y. Li, L. Jiang and Y. Zou, *Journal of Materials Chemistry C*, 2025, **13**, 15151-15158.
3. T. Lu, *The Journal of Chemical Physics*, 2024, **161**.
4. T. Lu and F. Chen, *Journal of Computational Chemistry*, 2012, **33**, 580-592.
5. J. Zhang and T. Lu, *Physical Chemistry Chemical Physics*, 2021, **23**, 20323-20328.